Published in final edited form as:
J Am Chem Soc. 2009 March 18; 131(10): 3631–3638. doi:10.1021/ja807680m.

Early Stages of Oxidative Stress-Induced Membrane Permeabilization: A Neutron Reflectometry Study

Hillary L. Smith[†], **Michael C. Howland**[‡], **Alan W. Szmodis**[§], **Qijuan Li**[‖], **Luke L. Daemen**[†], **Atul N. Parikh**[‖], and **Jaroslaw Majewski**[*,†]

†*Manuel Lujan Neutron Scattering Center, Los Alamos National Laboratory, Los Alamos, New Mexico 87545*

‡*Graduate Group of Chemical Engineering & Materials Science, University of California, DaVis, California 95616*

§*Graduate Group of Biophysics, University of California, Davis, California 95616*

‖*Graduate Group of Applied Science, University of California, Davis, California 95616*

Abstract

Neutron reflectometry was used to probe in situ the structure of supported lipid bilayers at the solid–liquid interface during the early stages of UV-induced oxidative degradation. Single-component supported lipid bilayers composed of gel phase, dipalmitoyl-*sn*-glycero-3-phosphocholine (DPPC), and fluid phase, 1-palmitoyl-2-oleoyl-*sn*-glycero-3-phosphocholine (POPC), phospholipids were exposed to low-dose oxidative stress generated by UV light and their structures were examined by neutron reflectometry. An interrupted illumination mode, involving exposures in 15 min increments with 2 h intervals between subsequent exposures, and a continuous mode involving a single 60 (or 90) min exposure period were employed. In both cases, pronounced differences in the structure of the lipid bilayer after exposure were observed. Interrupted exposure led to a substantial decrease in membrane coverage but preserved its total thickness at reduced scattering length densities. These results indicate that the initial phase during UV-induced membrane degradation involves the formation of hydrophilic channels within the membrane. This is consistent with the loss of some lipid molecules we observe and attendant reorganization of residual lipids forming hemimicellar edges of the hydrophilic channels. In contrast, continuous illumination produced a graded interface of continuously varied scattering length density (and hence hydrocarbon density) extending 100–150 Å into the liquid phase. Exposure of a DPPC bilayer to UV light in the presence of a reservoir of unfused vesicles showed low net membrane disintegration during oxidative stress, presumably because of surface back-filling from the bulk reservoir. Chemical evidence for membrane degradation was obtained by mass spectrometry and Fourier transform infrared spectroscopy. Further evidence for the formation of hydrophilic channels was furnished by fluorescence microscopy and imaging ellipsometry data.

Introduction

Oxidation of membrane lipids, such as following assaults by reactive oxygen species (ROS) produced during oxidative stress, has been implicated in a number of pathological conditions (e.g., aging,[1] Alzheimer's disease,[2] and apoptosis[3,4]). A significant body of literature now establishes the important role of changes to the membrane structure[5] and corresponding

E-mail: E-mail: jarek@lanl.gov.

Supporting Information Available: Detailed experimental procedures and mass spectroscopy data. This information is available free of charge via the Internet at http://pubs.acs.org/.

physical–chemical properties induced by lipid oxidation. Lipids of differing degrees of saturation respond differently to oxidative assault. For instance, unsaturated lipids are generally more prone to direct oxidation via rearrangement or loss of double bonds and in some instances the degradation of lipid tails. Some examples of membrane reorganizations following oxidation of lipids include changes in the packing of membrane components,[5] lateral fluidity,[6] domain reorganization[7,8] or molecular redistributions,[9] increased permeability,[10] and membrane phase behavior. Moreover, some of these membrane reorganizations may also influence the conformations and thus the functions of selected membrane proteins, which in turn characterize the pathological condition. Despite the progress these studies portend, our understanding remains poor of the early sequence of molecular events that trigger membrane remodeling following an oxidative assault as well as the fate of oxidation products, specifically their influence on the structure of the bilayer following membrane oxidation.

In this paper, we use neutron reflectometry (NR) to study the behavior of supported lipid bilayers under mild oxidative stress generated by short-wavelength UV light. Our choices for the model membrane configuration, characterization method, and oxidative stress-generating mechanism are influenced by the ease, versatility, and potential for molecular-level characterization. First, photogenerated reactive oxygen species provide an attractive means for generating controlled and localized oxidative stress. It is now well-established that illumination by short-wavelength UV radiation, such as that produced by 187 and 254 nm lines of simple Hg lamps, produces a highly reactive mixture of potent oxidants in water.[11] Specifically, a combination of singlet molecular oxygen, ozone, and even low concentrations of hydrogen peroxide can be controllably produced by varying the illumination period and proximity of the membrane structure to the source. Second, supported lipid bilayers, such as those formed by surface rupture and spreading of phospholipid vesicles,[12] provide a convenient means to produce membrane phases of desired chemical compositions and fluidity in a routine manner. These essentially planar, surface-supported membrane mimics are particularly suited to neutron reflection measurements for in situ characterization and also for controlled exposure to UV light. Third, simple contrast adjustment (e.g., replacing H_2O by D_2O), allows neutron reflection to offer a very precise means for probing sub-nanometer-scale changes to the hydrogenated membrane structure.[13]

Moreover, the use of UV light under certain conditions of exposures has recently been shown to allow complete removal of exposed lipids from the bilayer structure.[14,15] This approach allows a simple and direct route for patterning and compartmentalizing fluid lipid bilayers. However, the fate of oxidized lipids and the process by which oxidation is initiated remains poorly understood.

Experimental Section

Sample Preparations

Lipid bilayers are prepared by following the standard procedures for surface-induced rupture and spreading of small unilamellar vesicles (SUVs).[16] 1,2-Dipalmitoyl-*sn*-glycero-3-phosphocholine (DPPC) is dissolved to 0.5 mg/mL in chloroform and then dried under vacuum for 3 h. Lipids are rehydrated to 0.5 mg/mL in H_2O, heated to 50 °C, and sonicated with a probe-tip sonicator for 60 s at 100 W power. The warm solution is injected into the solid–liquid interface cell, which is heated on a hot plate. The solid–liquid interface cell[17] (Figure 1) is composed of a monocrystalline quartz slab against a Maycor ceramic piece (Ceramic Products, Inc., Palisades Park, NJ; containing SiO_2/MgO/Al_2O_3/K_2O/B_2O_3/F in the weight ratio 46:17:16:10:7:4) with a 0.2–0.3 mm air gap, sealed with an O-ring, and held in place with clamps and screws. The quartz crystal and Maycor piece are cleaned by rinsing with chloroform, 2-propanol, and ethanol, and placing in the UV ozone cleaner for 45 min. The solution of injected vesicles fills the gap between quartz and Maycor in the assembled solid–

liquid interface cell. The vesicles are allowed to fuse to the quartz and cool to room temperature for 1 h. Finally, the cell is carefully rinsed with D_2O, removing unfused lipid vesicles and leaving the bilayer behind. D_2O is used to provide neutron scattering contrast between quartz, hydrogenated lipids, and the bulk solution. The same protocol is followed for preparation of 1-palmitoyl-2-oleoyl-*sn*-glycero-3-phosphocholine (POPC) bilayers without heating the lipids or solid–liquid interface cell. In the case where unfused vesicles are present, this sample was created from incomplete rinsing of the vesicle solution. Surface coverage for this sample is not 100%, likely resulting from hydrophobic regions on the quartz where the bilayer did not form (see Results section for additional details).

Prior to UV illumination, the structure, coverage, and overall integrity of the target bilayer are characterized by neutron reflectometry (NR). A low-pressure Hg lamp housed in a quartz envelope is used as a source of short-wavelength UV (187–254 nm, 14 W, UVP Light Sources, Upland, CA). The lamp is placed ~20 mm from the bilayer. This distance is chosen to considerably limit the flux, allowing study of the initial stages of oxidative damage. A tent of aluminum foil is used to enclose the lamp and solid–liquid interface cell. The lamp is turned on for the prescribed exposure time and then turned off, and the sample is measured with NR. It is important to note that the sample was never disturbed between subsequent exposures and measurements; thus the footprint of the beam (~50 mm × 8 mm) remains constant in each experiment. All the NR experiments were performed at room temperature.

Neutron Reflectomery Experiments

Neutron reflectometry (NR) experiments were performed on the surface profile analysis reflectometer (SPEAR) at the Los Alamos National Laboratory Neutron Science Center (http://www.lansce.lanl.gov/lujan/instruments/SPEAR/index.html). SPEAR is a time-of-flight reflectometer with wavelengths λ = 2–16 Å on a polychromatic, pulsed neutron source. Monocrystalline quartz is chosen for its low neutron and UV absorption, and D_2O provides contrast against hydrogenated lipids. NR measurements are performed by measuring the ratio of reflected to incident intensity of a collimated neutron beam incident on the sample at a small angle, θ. This ratio is the reflectivity, R, and is measured as a function of the momentum transfer vector Q_z where $Q_z = (4\pi \sin \theta)/\lambda$ and λ is the neutron wavelength. The reflectivity data is multiplied by Q_z^4 and plotted versus Q_z to compensate for the sharp decrease in the reflectivity as described by Fresnel's law: $R \propto Q_z^{-4}$.[18]

The resulting reflectivity data is reduced by use of the incident neutron intensity spectrum. This data is compared to a model reflectivity profile generated from the Parratt recursion formalism[19] and the model is adjusted via genetic optimization to obtain the best least-squares fit by the Levenberg–Marquardt nonlinear least-squares method.[20] Our philosophy was to use the simplest possible model of physical relevance because limited maximum momentum transfer vector values restrict real-space resolution. In all cases, a one-slab model was used to describe the region containing the hydrogenated bilayer alkyl tails with the occasional addition of a second slab to describe the interface between the bilayer and bulk D_2O. This approach ignores the hydration layer known to exist at the quartz interface[21] and makes an approximation for the membrane to exclude lipid headgroups because the contrast of these regions is expected to be low as compared to the contrast provided by the hydrogenated alkyl tails. This simplification is supported by previous NR studies demonstrating that such approximations do not introduce significant errors[22] in the Q_z range measured. The scattering length density (SLD) distribution is described by a sequence of n slabs, each of constant scattering length density. Two adjoining layers i and $i + 1$ are connected by an error function centered at the interface to describe roughness between adjacent layers. Roughness includes contributions from static roughness and dynamic undulations.

Figure 2a shows a schematic of a bilayer at a quartz interface against a bulk D_2O subphase. It is drawn to scale with ~40 Å of the membrane's hydrogenated tails on top of a 5 Å water cushion. The SLD distribution shown in Figure 2b correlates directly to this schematic. The black curve represents the ideal SLD profile for a one-slab model of a tail region on a quartz substrate with no roughness between interfaces. The profile begins with the quartz slab at SLD 4.18×10^{-6} Å^{-2}, then introduces one slab extending ~40 Å in the *z*-direction with SLD -0.3×10^{-6} Å^{-2}, and ends with SLD of ~6.2×10^{-6} Å^{-2} for the bulk D_2O subphase. This profile is overlain with the fit to a real DPPC bilayer, shown in gray, which has the same characteristics as the black curve with the addition of roughness at each interface.

Attenuated Total Reflection Fourier Transform Infrared Spectroscopy

ATR-FTIR spectra were collected on a commercial Bruker Equinox 55 Fourier transform infrared spectrophotometer equipped with a horizontal ATR accessory (Harrick Scientific, Ossining, NY) and deuterated triglycine sulfate (DTGS) detector (Bruker, Göttingen, Germany). The mid-IR spectra in the frequency range 4000–600 cm^{-1} were obtained at a 4 cm^{-1} resolution for 60–400 scans by use of a Blackman Harris three-term apodization. The spectrophotometer was purged with dry air. UV-oxidized Si trapezoids, mounted in a boat configuration to allow liquid ambients, were used as the internal reflection elements (IREs). The number of active internal reflections in the IRE was $N = 10$. Data analysis was performed with commercial Grams 32 (Galactic Industries, Salem, NH) software.

Before use, the IREs were cleaned by a brief exposure to UV radiation followed by extensive rinsing in Millipore filtered water. Lipid bilayers were deposited onto IRE elements either by classical vesicle fusion method or by hydration of lipids spread from organic solvents onto the IRE.[23] The lipid-coated samples were subsequently exposed to UV radiation by use of low-pressure Hg pen-ray lamps (UVP, Inc.) encapsulated in a quartz tube for an extended duration (~90 min), and their spectra were recorded in real time. The longer durations were necessary because of the larger lamp–sample distances required by our illumination conditions and lower power achieved with the pencil lamps in real-time measurements. Spectra were recorded in continuous illumination mode.

Fluorescence Microscopy, Imaging Ellipsometry, and MALDI Mass Spectroscopy

Description of the experimental procedures used for these techniques are described in the Supporting Information. Conditions used were intended to closely match conditions used in the neutron experiments. Interpretation of the mass spectroscopy results are also found in the Supporting Information.

Results

For the first experiment set, DPPC bilayers are exposed to oxidative stress-generating UV (1) for a single 60 min exposure and (2) in increments of 15 min, to a cumulative exposure of 60 min, with 2 h measurements in between each exposure. Resulting reflectivity profiles and SLD plots are shown in Figure 2. In both cases, the SLD plots (Figure 2d,f) show an increase in SLD of the bilayer with exposure but little measurable change in membrane thickness. For a well-formed DPPC bilayer fused at the quartz–D_2O interface, the resulting SLD of the hydrogenated tails should be slightly less than 0.0×10^{-6} Å^{-2}. This value is calculated from the coherent scattering length of elements building the alkyl tails and the volume occupied by these tails. On the basis of the calculated SLD value, any changes in the fractional occupancy of lipids on the surface following UV exposure can be estimated by modeling a linear combination of the volumes of lipid tails and D_2O.

For the gradual exposure data in Figure 2c,d, the reflectivity is described with a one-slab model in which the coverage of DPPC on the surface gradually decreases from 100% before exposure to 93% after 15 min, 91% after 30 min, 85% after 45 min, and 68% after 60 min. This change in coverage corresponds to an average rate of decrease of 0.5%/min. Figure 2e,f summarizes single-exposure data. These data cannot be adequately described with a single slab at the quartz interface, as in the case of gradual exposure. Fitting of NR data requires introduction of a new region adjacent to the membrane and extending into the bulk solution. This region is much thicker than the membrane and extends approximately 150 Å into the bulk solution. The SLD of this region is 5.5×10^{-6} Å^{-2} at the membrane interface and gradually increases to the SLD of the bulk solution. Further, the integrated SLD of this new region is almost equal to the integrated decrease of the SLD in the lipid membrane region, which may suggest the conservation of hydrogenous material in the system. Estimates of coverage of the membrane show a decrease from 100% to 83% over 60 min of exposure time, amounting to a decrease at a rate of 0.3%/min.

A second set of experiments was performed on a DPPC bilayer with excess vesicles adsorbed to the bilayer interface. This sample is obtained by limiting rinsing of the vesicle solution after bilayer formation (see Experimental Section for details). In this case, the underlying target bilayer occupies approximately 80% of the surface. The reflectivity profile confirms the essential features of this configuration; specifically, the presence of unfused vesicles is revealed by small fringes at low Q_z, indicative of a long length scale (Figure 3a,b). These fringes correspond in the SLD profile to an additional slab extending 600 Å into the D_2O subphase. During exposure to UV in increments of 15 min, (i) the thickness of the membrane remains constant; (ii) the extended region at the membrane interface dissipates; and (iii) the SLD of the membrane region remains relatively constant, corresponding to its initial coverage of ~80%.

A third set of experiments examines oxidative stress-induced changes in the behavior of the unsaturated lipid POPC. Bilayers of POPC were exposed to UV (1) in increments of 15 min, up to a cumulative 60 min exposure, and (2) for a single 90 min exposure. Results are similar to those obtained with bilayers of DPPC. In both cases, SLD increases with exposure and the thickness of the bilayer remains constant (Figure 4b,d). The increase in SLD corresponds to a decrease in coverage of POPC on the substrate. Initial membrane coverage is ~100%, reducing to 92% after 15 min, 78% after 30 min, 52% after 45 min, and 47% after 60 min. This change in coverage corresponds roughly to an average rate of decrease of 1.0%/min. For single exposure, the coverage decreases from 100% to 40% after 90 min, corresponding to an average rate of 0.7% per minute. As in the DPPC case, the single long exposure introduces a graded interface region, as indicated by the requirement of an additional slab to adequately fit the data. In this case, the graded interface region begins at 5.85×10^{-6} Å^{-2} and reaches the bulk SLD at 6.2×10^{-6} over approximately 100 Å. Favorable contrast conditions between the remains of the POPC bilayer and the graded interface region make it possible to see the latter with NR, as evidenced by an additional interference fringe with a minimum at ~0.075 Å^{-1} in Q_z (Figure 4c).

The fourth set of experiments repeated UV exposures of DPPC and POPC bilayers where the pure D_2O subphase was replaced with 0.1 M solutions of known antioxidants, D-mannitol and L-ascorbic acid.[24,25] During single exposure of a POPC membrane in the presence of L-ascorbic acid, the coverage decreased only 8% in 60 min at an average rate of 0.13%/min. For DPPC membranes, L-ascorbic acid slowed the average rate of decrease in membrane coverage for gradual exposure to 0.2%/min and slowed continuous membrane exposure to 0.26%/min. Measurements with D-mannitol solution proved unreliable in comparing membrane coverage because exposure populated the surface with microbubbles.

FTIR experiments were performed to examine the change in chemical structure of wet DPPC during UV-induced oxidative stress. Results summarized in Figure 5 show the exposure dependent variations in characteristic peaks associated with methyl (2873 and 2956 cm^{-1}), methylene (2850 and 2918 cm^{-1}), and carbonyl (1738 cm^{-1}) vibrational mode absorptions. All three peaks display continuous and gradual decay in integrated intensities following UV exposure (Figure 5b), consistent with corresponding removal of material from the surface. [The precise value of the intensity depends on both the vibrational mode cross-sections of degradation products and their surface occupancies. As a result, a quantitative determination of the loss of material is not possible.].

Discussion

These experiments attempt to understand the effects of oxidative stress in its very early stages of assault on the membrane. We have targeted specific membrane components, saturated and unsaturated lipid types, and studied two modes of oxidative attack, continuous and interrupted, to distinguish how these different characteristics impact bilayer integrity and composition under oxidative stress. An additional case was also introduced to study the influence of a reservoir of unfused vesicles on the membrane during exposure. From these results we can draw conclusions about UV-induced structural perturbations in the lipid bilayer, develop plausible models for oxidative reorganization, and elucidate the dependence of these mechanisms on chain saturation and mode of oxidative attack.

Photoinduced Oxidative Stress Produces Membrane Permeabilization and Pore Formation

The first significant results to consider are that (i) bilayer thickness remains constant as a function of oxidative stress and (ii) membrane scattering length density increases with increasing exposure time. The increasing SLD allows calculations of membrane coverage as a function of oxidative stress and average rates of decrease in coverage, as discussed above. Additionally, independent verification of loss of material in the membrane was obtained by FTIR and mass spectroscopy. Gradual and continuous loss of infrared absorption intensities due to methylene, methyl, and carbonyl vibrational modes, as seen with FTIR, suggests that fragments of these materials are being lost from the surface. Comparison of the spectra for control and exposed samples obtained with matrix-assisted laser desorption/ionization (MALDI) mass spectroscopy show that the signature for the intact DPPC molecule has virtually disappeared in the exposed case (see spectra in Figure S1 of the Supporting Information). Also, the appearance of new peaks suggests cleavage of the headgroup from the tail. The presence of numerous smaller fragments is consistent with further fragmentation of the lipid tails. From these observations it is clear that the membrane degrades gradually over time. This loss of membrane material must produce energetically unfavorable densities within the bilayer. Because the resultant membrane coverage following the oxidative degradation is significantly lower than that required for membrane lysis (~2–8%),[26] it seems reasonable that the bilayer undergoes molecular rearrangements in response to the changing balance of van der Waals, hydration, and hydrophobic forces. These rearrangements lead to effective permeabilization of the membrane bilayer by creating D_2O-filled hydrophilic pores (Figure 6). Such formation of water channels is a generic mechanism seen in biological membranes experiencing electrical or physiological attack or when viral interactions occur.[27,28] The formation of pores in the membrane is further supported by wide-field fluorescence microscopic measurements. Here, single POPC bilayers doped with 1 mol % Texas red-conjugated DHPE lipid is exposed to UV for 3 min. Short exposure times used in these experiments were necessary to match conditions of 30–60 min time intervals in NR and FTIR measurements because of the use of a high-intensity grid lamp in closer proximity to the sample surface as compared with the lower power pen lamp required for FTIR and neutron reflectivity experiments. These results, summarized in Figure 7, clearly show the appearance of numerous randomly distributed black spots several

micrometers wide. Further characterization of these nonfluorescent features by imaging ellipsometry data confirms the loss of material from the membrane during UV irradiation (data not shown).

Prolonged Stress Forms Stable Graded Interface

The second significant result is the development of the graded interface during continuous oxidative assault (as opposed to interrupted). This new region, required to adequately fit the data in cases of both continuous exposure of DPPC and POPC, is more than 3 times the thickness of the membrane itself and has considerable roughness, creating a gradient to the bulk solution. The SLD of this region is lower than D_2O but greater than that of the membrane. This suggests the presence of either hydrogenated residues or air bubbles, though it is unlikely that air bubbles of this size would be stable at the interface and survive the high Laplace pressure. Thus, a plausible explanation is that lipid fragments in the proximity of the membrane occupy this region. We do not understand the mechanism leading to formation of this region and why this region is easily discerned in the case of continuous exposure but not apparent in the interrupted one. A graded interface may exist in the case of interrupted exposure as well, but because less material is lost and an additional slab in this region would have an SLD very close to that of water, it would not be detected due to lack of contrast.

Together, these two results help to describe the early stages of oxidative assault when the membrane maintains structural integrity. This description of the UV-induced structural perturbations and the model for oxidative reorganization then lend themselves to understanding the membrane behavior when a reservoir of excess vesicles is present on the surface of the target bilayer during oxidative assault.

Excess Vesicles Minimize Membrane Deterioration during Oxidative Assault

The third significant result is seen during photoillumination in the presence of a reservoir of unfused vesicles. The unexposed SLD profile exhibits two length scales consistent with (i) a bilayer occupying 80% of the surface and (ii) unfused vesicles. During oxidative assault, the membrane thickness, SLD, and coverage remain surprisingly constant despite incomplete membrane coverage before assault. The large length scale dissipates, indicating that the vesicle reservoir is no longer present. One plausible explanation for this result is that normal oxidative assault occurs on the membrane, via the process described earlier; however, the unfused vesicles act as a source of lipids to repopulate regions of the membrane depleted from the oxidative degradation and perhaps shield the bilayer from further oxidative damage.

Chain Saturation and Mode of Photoillumination Influences Oxidative Damage

Further information about how oxidative damage occurs is gleaned from comparison of average rates of decrease in membrane coverage. While these exact values are subject to many experimental considerations, the trend in these rates is instructive. First, the rate of decrease in surface coverage is 20–30% faster with interrupted exposure than continuous exposure. This effect can be explained by oxidized membrane materials remaining in proximity to the membrane, as seen by the graded interface in the case of continuous exposure, and thus shielding the underlying membrane from further oxidation. Second, coverage decreases faster for the unsaturated lipid POPC than saturated DPPC. These results are expected from the lower packing density of POPC lipids, which accelerates the diffusion rate of reactive oxygen species within the membrane. Moreover, the presence of double bonds also makes POPC far more susceptible to oxidative attack than saturated lipids below their transition temperature.

ROS Scavengers Minimize Membrane Degradation

The introduction of scavengers of reactive oxygen species into the subphase during oxidative assault slowed the average decrease in membrane coverage as a function of exposure in experiments of both gradual and continuous exposure of DPPC and POPC membranes. These scavengers have been previously demonstrated to mitigate the effects of oxygen radical-generated damage on DNA.[24,25] The most pronounced effect was visible in POPC membranes, which is expected because POPC is in the fluid phase at room temperature while DPPC is in the gel phase. For a POPC membrane, the 0.1 M solution of L-ascorbic acid virtually halted membrane degradation, slowing the average rate of decrease in membrane coverage by 81% to 0.13%. For DPPC membranes, L-ascorbic acid slowed the average rate of decrease in membrane coverage for gradual exposure by 60% and slowed continuous exposure degradation by approximately 13%. The effect of this antioxidant in mitigating membrane damage provides further evidence for UV-generated ROS in solution.

Conclusion

Using a model configuration of supported lipid bilayers at the solid–liquid interface, UV-generated oxidative stress, and NR to probe the structure of the system, we mimic the very early stages of oxidative assault on a lipid biomembrane. We conclude that, during early phases of membrane degradation, the net molecular membrane density decreases while residual material maintains a normal bilayer motif. These two results in conjunction with models of membrane lysis are reconciled by membrane permeabilization due to water channel formation. NR also detects an unusual graded interface at the membrane–water interface during continuous exposure. We hypothesize that the composition of this extended interface region appears to be a gradient of oxidized material into bulk solution. When a lipid reservoir, in the form of unfused vesicles in proximity to the membrane, is present, we find a measurably reduced rate of membrane oxidation. This is consistent with membrane repopulation afforded by the lipid reservoir. Finally, unsaturated lipids oxidize faster than saturated lipids, as indicated by faster rate of decrease in coverage in the former case, and the presence of antioxidant L-ascorbic acid slows the rate of decrease in coverage in all cases.

Supplementary Material

Refer to Web version on PubMed Central for supplementary material.

Acknowledgments

This work was supported by Los Alamos National Laboratory under DOE Contract W7405-ENG-36, DOE Office of Basic Energy Science. Support for this work was provided by a grant from BES, Department of Energy under Award DE-FG02-04ER46173. A.W.S. is supported by Student Fellowships (UEPP and SEGRF) from Lawrence Livermore National Laboratory, and M.C.H. is supported by Grant T32-GM08799 from NIGMS-NIH. We thank Timothy Sanchez and Srinivas Iyer for assistance with mass spectroscopy measurements.

References

1. Hsiai T, Berliner JA. Curr Drug Targets 2007;8(12):1222–1229. [PubMed: 18220699]
2. Markesbery WR, Carney JM. Brain Pathol 1999;9(1):133–146. [PubMed: 9989456]
3. Martinet W, Kockx MM. Curr Opin Lipidol 2001;12(5):535–541. [PubMed: 11561173]
4. Spiteller G. Physiol Plant 2003;119(1):5–18.
5. Megli FA, Russo L. Biochim Biophys Acta 2008;1778(1):143–152. [PubMed: 18054893]
6. Kaplan P, Racay P, Lehotsky J, Mezesova V. Neurochem Res 1995;20(7):815–820. [PubMed: 7477674]
7. Ayuyan AG, Cohen FS. Biophys J 2006;91(6):2172–2183. [PubMed: 16815906]

8. Samsonov AV, Mihalyov I, Cohen FS. Biophys J 2001;81(3):1486–1500. [PubMed: 11509362]
9. Megli FM, Russo L, Sabatini K. FEBS Lett 2005;579(21):4577–4584. [PubMed: 16098528]
10. Vercesi AE, Kowaltowski AJ, Grijalba MT, Meinicke AR, Castilho RF. Biosci Rep 1997;17(1):43–52. [PubMed: 9171920]
11. Sanii B, Parikh AN. Annu Rev Phys Chem 2008;59:411–432. [PubMed: 18031214]
12. Tamm LK, Mcconnell HM. Biophys J 1985;47(1):105–113. [PubMed: 3978184]
13. Krueger S, Meuse CW, Majkrzak CF, Dura JA, Berk NF, Tarek M, Plant AL. Langmuir 2001;17(2):511–521.
14. Yee CK, Amweg ML, Parikh AN. J Am Chem Soc 2004;126(43):13962–13972. [PubMed: 15506757]
15. Yee CK, Amweg ML, Parikh AN. Adv Mater 2004;16(14):1184–+.
16. Brian AA, Mcconnell HM. Proc Natl Acad Sci U S A 1984;81(19):6159–6163. [PubMed: 6333027]
17. Doshi DA, Dattelbaum AM, Watkins EB, Brinker CJ, Swanson BI, Shreve AP, Parikh AN, Majewski J. Langmuir 2005;21(7):2865–2870. [PubMed: 15779959]
18. Als-nielsen J. Physica A 1986;140(1–2):376–389.
19. Parratt LG. Phys Rev 1954;95(2):359–369.
20. Nelson A. J Appl Crystallogr 2006;39:273–276.
21. Sackmann E. Science 1996;271(5245):43–48. [PubMed: 8539599]
22. Majewski J, Wong JY, Park CK, Seitz M, Israelachvili JN, Smith GS. Biophys J 1998;75(5):2363–2367. [PubMed: 9788931]
23. Seul M, Sammon MJ. Thin Solid Films 1990;185(2):287–305.
24. Anderson D, Yu TW, Phillips BJ, Schmezer P. Mutat Res 1994;307(1):261–271. [PubMed: 7513806]
25. Pelle E, Huang X, Mammone T, Marenus K, Maes D, Frenkel K. J InVest Dermatol 2003;121(1):177–183. [PubMed: 12839579]
26. Lipowsky, R.; Sackmann, E. Structure and Dynamics of Membranes: Generic and Specific Interactions. Vol. 1. Vol. 1B. Elsevier Science B. V.; Amsterdam: 1995.
27. Needham D, Hochmuth RM. Biophys J 1989;55(5):1001–1009. [PubMed: 2720075]
28. Brogden KA. Nat Rev Microbiol 2005;3(3):238–250. [PubMed: 15703760]

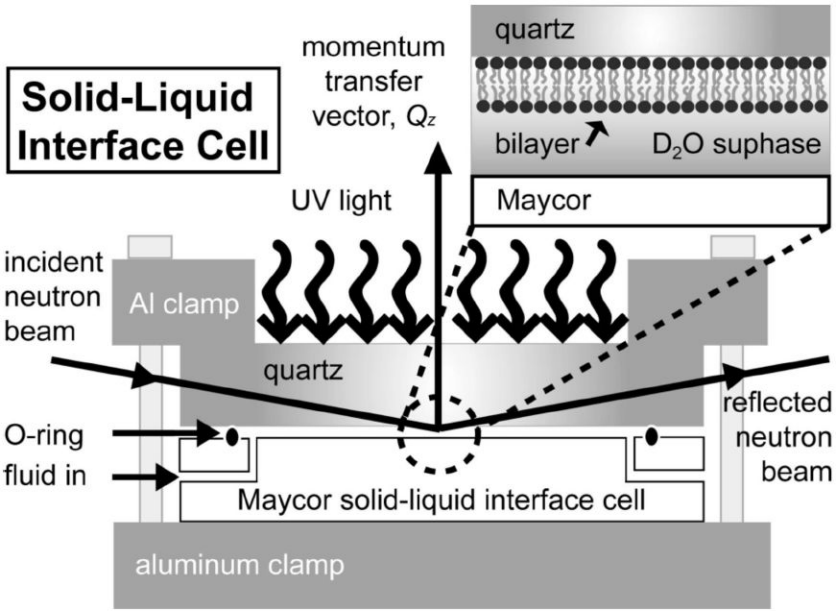

Figure 1.

Schematic of the solid–liquid interface cell used in neutron reflectometry measurements. A quartz slab is clamped against a Maycor piece with a 0.2–0.3 mm gap for fluid. The neutron beam penetrates through the lateral face of the quartz slab to reach the interface where the target bilayer resides. Illumination by UV light occurs through the quartz slab. Absorption of UV light at wavelengths 187 and 254 nm through the 10 mm thick monocrystalline quartz used in these experiments is 76% and 45%, respectively.

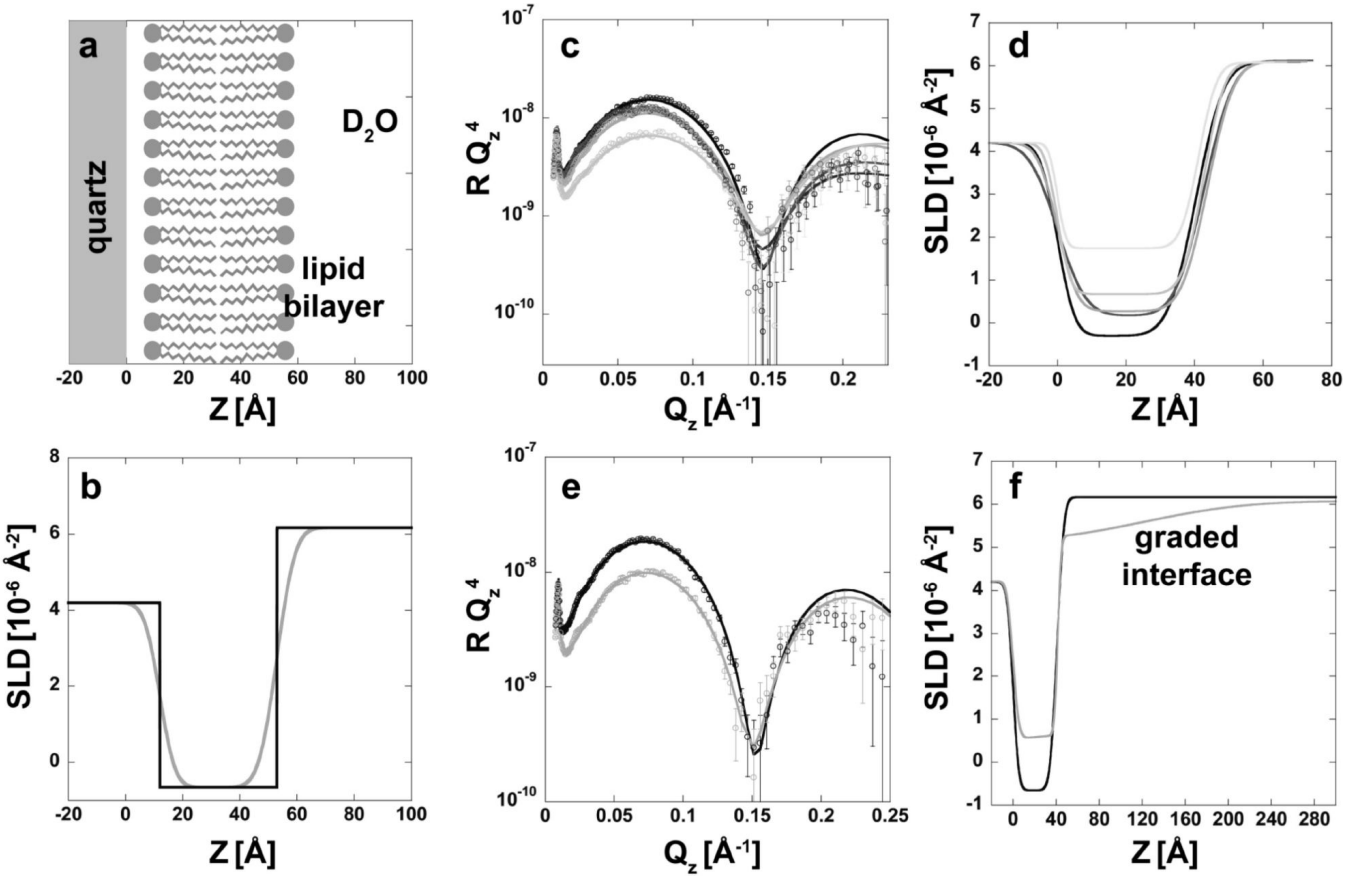

Figure 2.

(a) Lipid bilayer membrane at the quartz–D_2O interface; (b) corresponding model of the SLD distribution of this membrane using a one-slab model. Gray and black profiles show the SLD distribution with and without accounting for roughness at the interfaces, respectively. Similar profiles have been used to fit to the data for pure DPPC or POPC bilayers in the incremental exposure experiments. (c, e) Neutron reflectivity data obtained for incremental and single exposure of DPPC bilayers to UV, respectively; (d, f) corresponding SLD profiles. In panels c–f, increasing exposure time is shown in decreasing shades of gray, with no UV exposure in the darkest color. In both cases, the bilayer thickness remains constant with exposure and the SLD increases, indicating a decrease in bilayer coverage. Modeling of the single-exposure data requires an extra slab resulting in a graded interface region as seen in panel f.

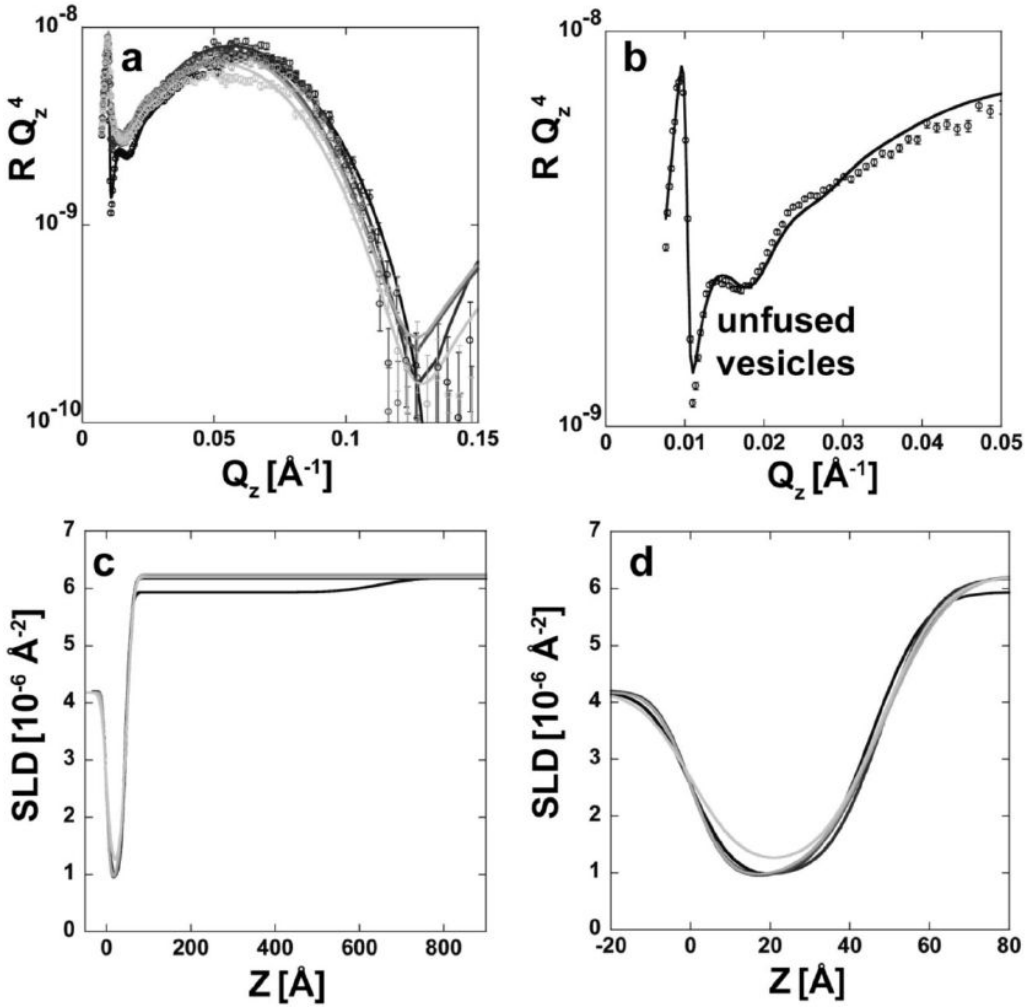

Figure 3.

(a) Neutron scattering profiles for incremental UV exposure of the DPPC bilayer with the reservoir of unfused vesicles; (c) corresponding SLD profile obtained from the fitting procedure. (b) Enlargement of the region at low Q_z where the signature of unfused vesicles is present, as indicated by the small fringes; (d) enlargement of the membrane region only, demonstrating almost no change in SLD of the bilayer. In all plots, increasing exposure time is shown in decreasing shades of gray, with no UV exposure in the black traces.

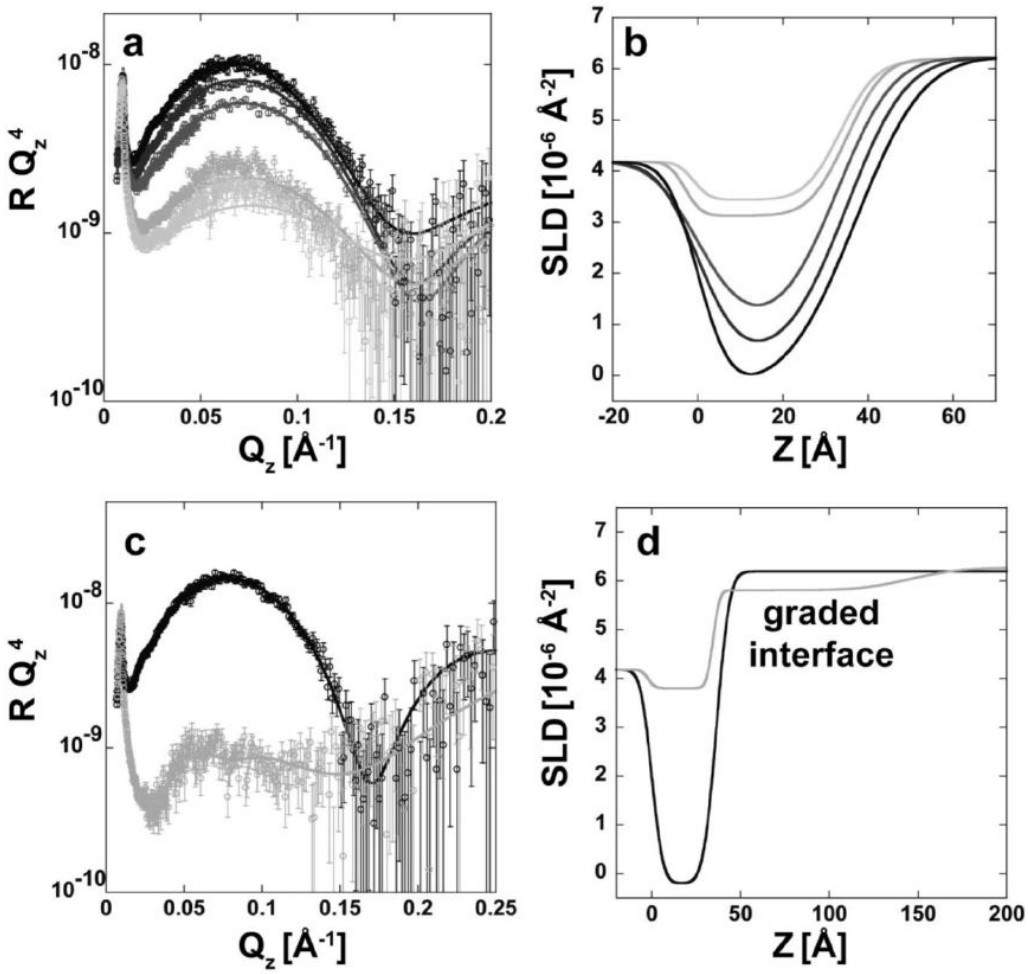

Figure 4.

(a, c) Neutron reflectivity profiles obtained for incremental and single exposure of POPC bilayers to UV, respectively; (b, d) corresponding SLD profiles. In all plots, increasing exposure time is shown in decreasing shades of gray, with no UV exposure for the black traces. In both cases, bilayer thickness remains constant with exposure and SLD increases, indicating a decrease in bilayer coverage. Note that the rate of decrease in coverage in the case of POPC is substantially higher than in the case of DPPC. Modeling of the single-exposure data requires an extra slab resulting in a graded interface region as seen in panel d.

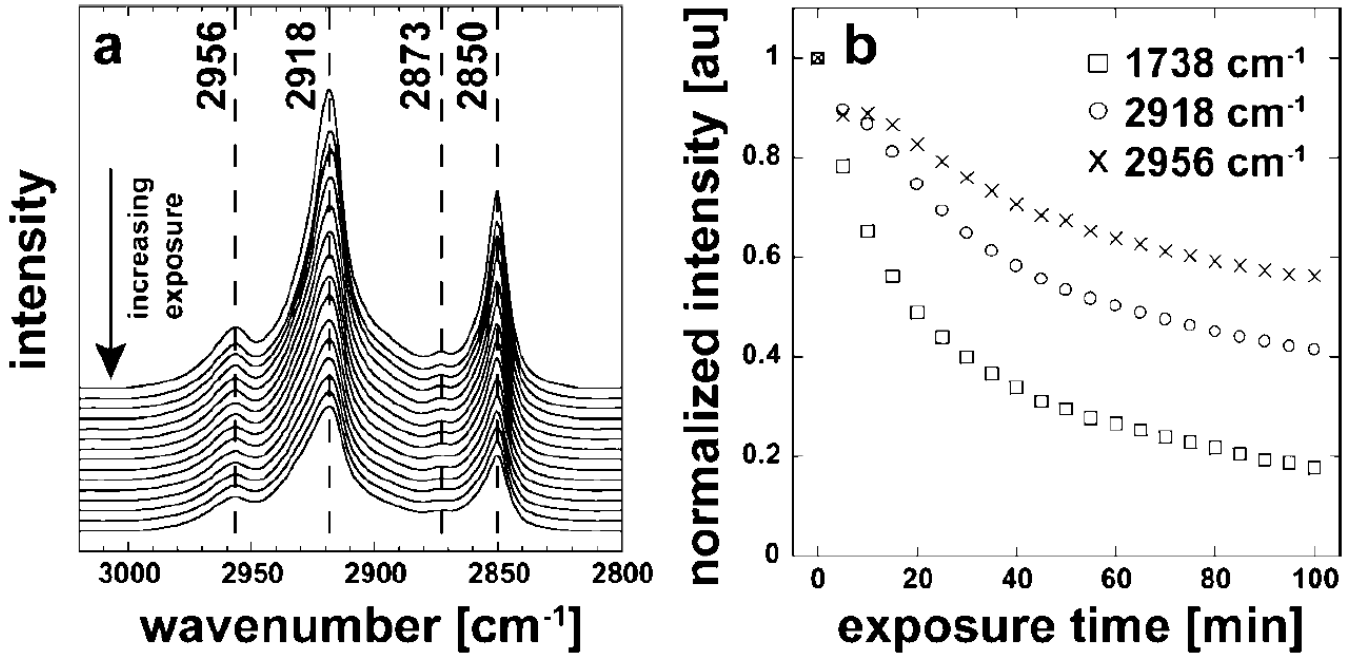

Figure 5.

(a) FTIR spectra for a single DPPC bilayer, acquired at 5–10-min intervals during exposure to UV. The arrow indicates the direction of increasing exposure time, in increments of 5 min to a cumulative 40 min and in increments of 10 min to a cumulative 100 min. (b) Decreasing integrated intensity of three peaks as a function of time. (○) Methylene absorptions, 2918 cm^{-1}; (×) methyl absorptions, 2956 cm^{-1}; (□) carbonyl absorptions, 1738 cm^{-1}. Decreasing intensity indicates that degradation is continuous throughout exposure.

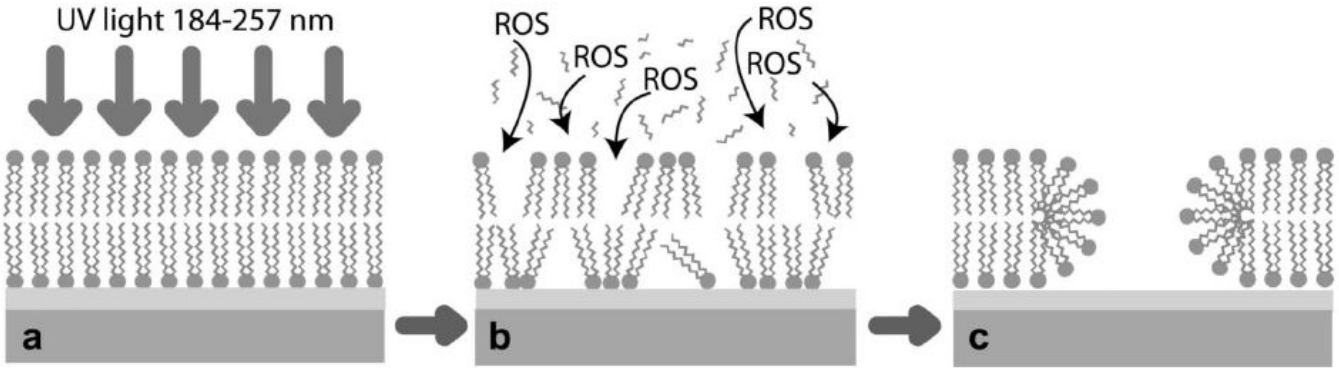

Figure 6.
Schematic of the oxidation process occurring during exposure of the bilayer to UV. (a) The membrane is exposed to UV in the range λ = 184–257 nm. (b) Reactive oxygen species (ROS) enter the membrane and lipid fragments enter solution. (c) The membrane is rearranged to yield pores where D_2O enters.

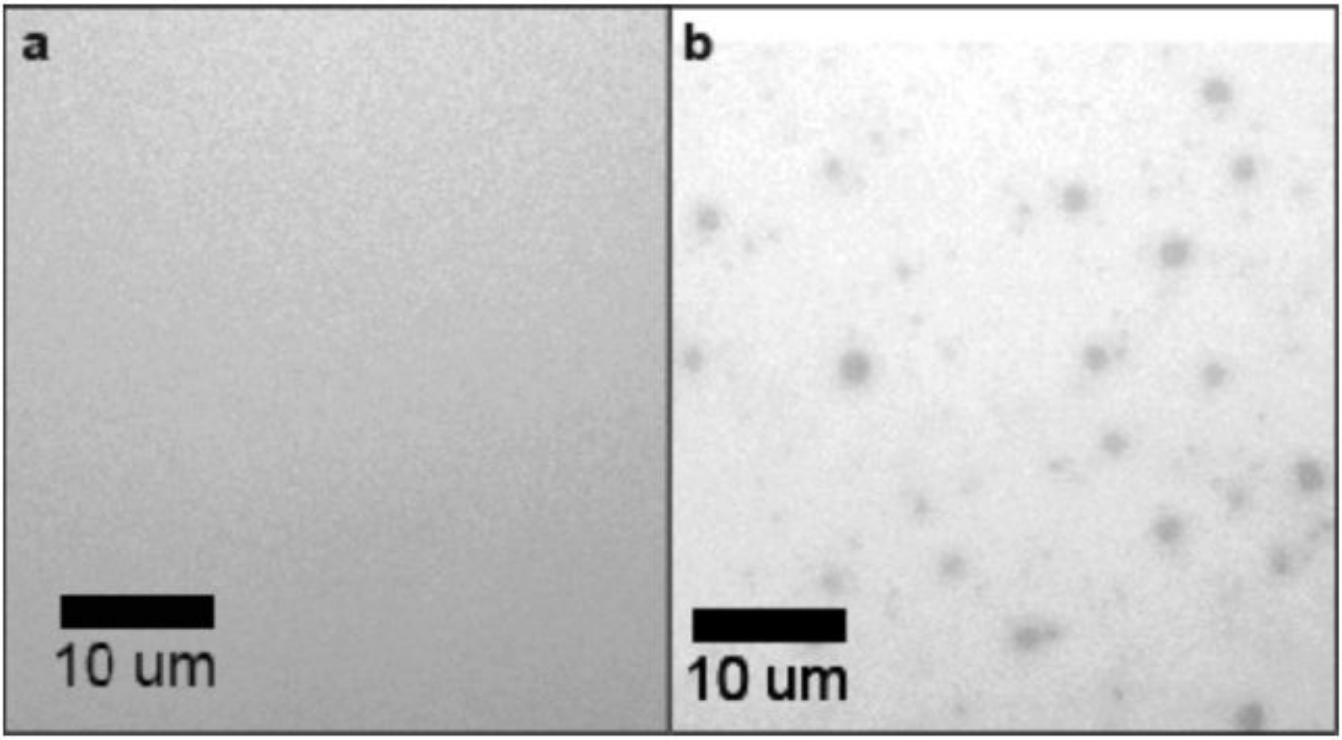

Figure 7.
(a) Fluorescent micrographs were collected of a POPC bilayer, deposited via vesicle fusion, containing 1% Texas Red DHPE. (b) The bilayer was exposed to UV for 3 min and reimaged. After this UV exposure period, black spots appear in the membrane, indicative of the formation of pores.